E19-2015-98

E. B. Dushanov [*], N. A. Koltovaya

COMPARISON OF MODELING STRUCTURES
OF WILD-TYPE HOMODIMER AND MUTANT HETERO-
AND HOMODIMERS OF PHOSPHATASE *hITPA*-**P32T**

[*] E-mail: dushanov@jinr.ru

Душанов Э. Б., Колтовая Н. А.   E19-2015-98

Сравнение модельных структур гомодимера дикого типа
и мутантных гетеро- и гомодимеров фосфатазы *hITPA*-P32T

Для выявления конформационных изменений, обуславливающих инакти-
вирующее действие мутации P32T инозин трифосфат пирофосфатазы чело-
века (*hITPA*), проведен анализ нескольких модельных структур. Конформа-
ция мутантного протомера отличалась от кристаллической структуры мутант-
ного апофермента (PDB: 4F95), а конформация протомера дикого типа — от
кристаллической структуры холофермента дикого типа (PDB: 2J4E). Между мо-
делированными структурами ферментов дикого и мутантного типов наблюдались
различия на трех участках: двух петлях и C-конце. Петля между $\alpha1$ и $\beta2$ (28–
33 а. о.), включающая сайт локализации мутантного аминокислотного остатка
Phe31-Pro32Thr-Cys33, в протомерах двух типов (дикого и мутантного) имела
две конформации, характеризующиеся разным положением соседней боковой
группы Phe31. Эти конформации стабильны. В кристаллической структуре
мутантного гомодимерного апофермента наблюдалось выворачивание в раствор
гидрофобного остатка Phe31.

Работа выполнена в Лаборатории радиационной биологии ОИЯИ.

Препринт Объединенного института ядерных исследований. Дубна, 2015

Dushanov E. B., Koltovaya N. A.   E19-2015-98

Comparison of Modeling Structures of Wild-Type Homodimer
and Mutant Hetero- and Homodimers of Phosphatase *hITPA*-P32T

The modeling structures of human inosine triphosphate pyrophosphatase (*hITPA*)
were analysed to identify conformational changes induced by inactivation effects of
P32T mutations. The conformation of the mutant protomer differed from the crystal
structure of mutant apoenzyme (PDB: 4F95), and that of the wild-type protomer
differed from the crystal structure of wild-type holoenzyme (PDB: 2J4E). Mutant
model differed from wild-type model in three regions: two loops and a C-terminal
region. The loop between $\alpha1$ and $\beta2$ (28–33 res.), including the site of localiza-
tion of mutant amino acid residue Phe31-Pro32Thr-Cys33, in wild-type and mutant
protomers had two conformations characterized by different positions of the Phe31
side group. These conformations were stable. In the crystal structure of the mutant
homodimer apoenzyme, the hydrophobic residue Phe31 was seen to go into solution.

The investigation has been performed at the Laboratory of Radiation Biology,
JINR.

Preprint of the Joint Institute for Nuclear Research. Dubna, 2015

INTRODUCTION

Under physiological conditions nucleotides suffer chemical modifications. The main type of chemical modification of purines is deaminization of purine bases. The C6 deaminization of adenine or C2 deaminization of guanine results in the formation of hypoxanthosine or xanthosine, respectively. Hypoxanthosine as a part of a nucleotide, i.e., hypoxanthosine riboside, is referred to as inosine. In addition, non-canonical bases are synthesized during the purine metabolism. Non-canonical nucleotides can accumulate in the pool of nucleotides and be included in the DNA and RNA, changing the genetic information and structure of nucleic acid. Living organisms have specific enzymes (nucleoside triphosphate pyrophosphohydrolases) for hydrolysis of these non-canonical nucleoside triphosphates to nucleoside monophosphates and pyrophosphates, thus removing them from metabolic processes.

The structure of inosine triphosphate pyrophosphohydrolase has been studied in several organisms among archaea, bacteria, and eukaryotes (Table 1). For example, the enzyme is encoded by the *RdgB* gene in bacteria *E. coli*, the *HAM1* gene in yeast *S. cerevisiae*, and the *hITPA* (human Inosine Triphosphate PyrophosphatAse) gene in human. These structures show a remarkable degree of conservation of the tertiary structure. Structural similarities indicate that *ITPA* and its homologs perform an important and evolutionarily conserved function. In all cases the protomers in the dimer are related by a 2-fold symmetry axis. The *hITPA* is a homodimer. Protomer is composed of 194 amino acids and consists of a large central β sheet forming the floor of the active site, with two mainly α-helical lobes flanking the active site (upper and lower lobes). The substrate binds in the cleft between the two lobes (Fig. 1). Each protomer has an independent active site for the Mg^{2+} ion and the ITP substrate binding. The phosphatase complex forms via hydrogen bonds of the upper lobes of each protomer.

The *hITPA*-P32T mutation rather often occurs in humans and can affect sensitivity of patients to medicines [3]. The mutation is located in the lower lobe. The mechanism for the inactivating effect of the mutation is not known. Two hypotheses were put forward [2, 4], which assume that the changes took place either in the interaction of the upper lobes of the monomers, affecting the formation of the dimer, or in the lower lobes in the mutant loop, which led to uncovering of the hydrophobic site. However, the wild-type and P32T forms were dimeric in

Table 1. List of nucleotide triphosphate pyrophosphatases in PDB

Code	Object	Resolution, Å	Organism	Reference
Inozine triphosphate pyrophosphatase				
2CAR	Apoprotein	1.09	Homo sapience (*ITPA*)	[4]
2J4E	1 polymer, 4 ligands	2.80	Homo sapience (*ITPA*)	[4]
2I5D	Apoprotein	1.63	Homo sapience (*ITPA*)	[8]
4F95	Apoprotein P32T	2.07	Homo sapience (*ITPA*)	[2]
1K7K	Apoprotein	1.50	Bacteria *E.coli* (*RdgB* ortholog *ITPA*)	[9]
2Q16	Apoprotein + ITP	1.95	Bacteria *E.coli* (*RdgB* ortholog *ITPA*)	[9]
Xanthosine triphosphate pyrophosphatase/Ham1 protein homolog				
1VP2	Apoprotein	1.78	Bacteria *Thermotoga maritima*	[10]
Nucleotide triphosphate pyrophosphatase				
2E5X	Polymer + ITT	2.00	Anaerobic archaeon *Pyrococcus horicoshi*	[11]
1B78	Polymer	2.20	Thermostable bacteria *Methanococcus jannaschii* (substrate ITP/dITP, XTP)	[12]
2MJP	Pyrophosphatase + 5'-Adenel-Imido-Triphosphate	2.20	Thermostable bacteria *Methanococcus jannaschii* (substrate ITP/dITP, XTP)	[12]
Non-canonical purine NTP pyrophosphatase				
4BNQ	Polymer	2.28	Bacteria *Staphylococcus aureus subsp. aureus*	[13]

solution and in crystal structure [5]. This abolishes the previous speculation that the P32T change disrupts dimerization as a mechanism of inactivation. Biochemical analysis of enzyme activity gave ambiguous results. The observation that individuals heterozygous for the P32T mutation retained 22.5% ITPase activity and homozygotes have an undetectable activity [6] suggested that both protomers of the physiological dimer need to be intact for catalytic activity. *In vitro* purified *ITPA*-P32T had enzymatic activity similar to the wild-type enzyme, indicating that the loss of activity in erythrocytes *in vivo* was indirect [5]. However, in another work the ITPase-P32T had 55% activity with ITP compared to wild-type ITPase [7]. So, the question was left open.
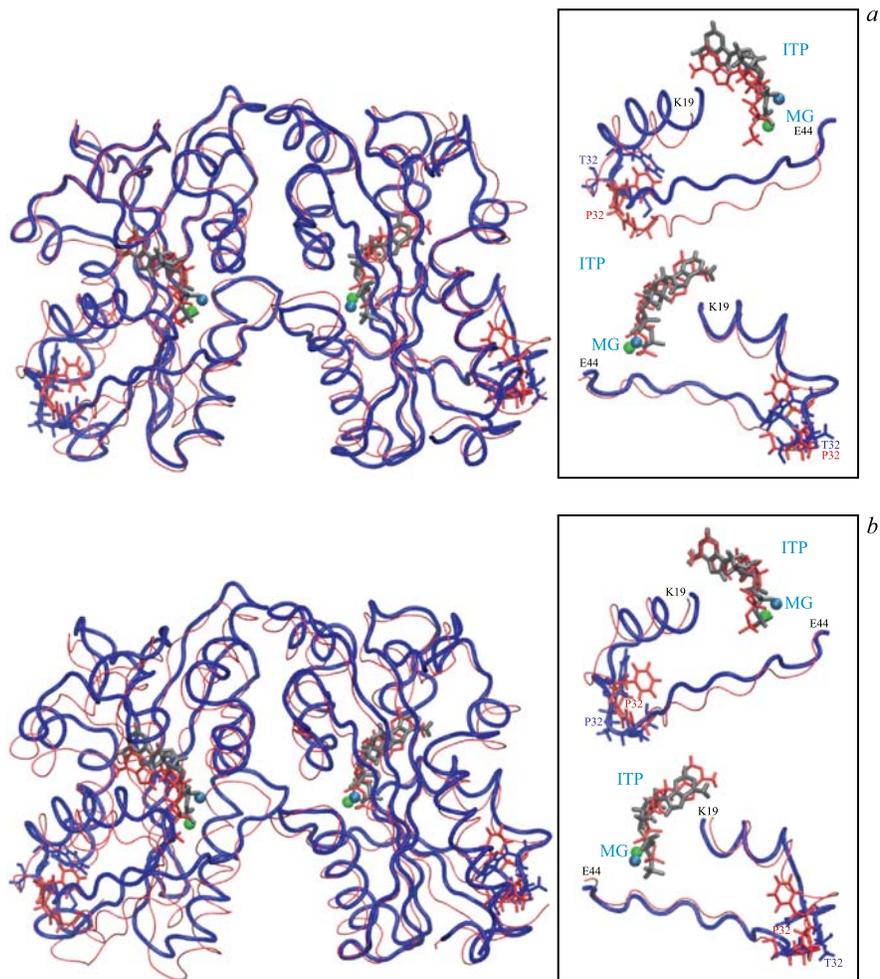
Fig. 1. Superpositions of relax (3 ns) structures of wild-type dimer (blue) with mutant homodimer (*a*, red) and mutant homodimer (*b*, red). A zoomed view of the area near mutant site P32/T32 is given in boxes

For *hITPA*, the PDB (Table 1) contains several high-resolution crystal structures of the so-called apoenzyme (active site free of bound molecules) and its complexes with low-molecular ligands, for example, the apoenzyme with a resolution of 1.1 Å (PDB code 2CAR; [4]) and 1.63 Å (PDB code 2I5D; [8]), and a structure of the complex with the physiological substrate ITP with a resolution of 2.8 Å (PDB code 2J4E; [4]). For the mutant, a crystal structure of the apoenzyme

3

with a resolution of 2.07 Å was obtained (PDB code 4F95; [2]). For the mutant heterodimer, there is no crystal structure.

To verify the above hypotheses, we earlier simulated structures of three forms of the enzyme (wild-type, mutant homodimer, mutant heterodimer) using computer dynamic simulation [1]. In this paper, simulation techniques and the changes in three forms of the enzyme during computer modeling were described. The initial geometry of the complex was specified in accordance with the lattice obtained from the X-ray structure analysis (PDB code 2J4E). In the present paper, we perform a comparative analysis of the simulated 3 ns forms of the enzyme.

1. RESULTS

The results of the simulation and 3D images of the *hITPA* protein complex were analyzed using the codes RasMol [14], MOLMOL [15], and Visual Molecular Dynamics (VMD) [16].

Earlier the structure of mutant protein forms was simulated using the crystal structure of the holoenzyme (PDB accession code 2J4E; [4]). Apart from two protomers, the enzyme comprised the cofactor, two Mg^{2+} ions and substrate — two molecules of ITP. The protomers in the dimer were different in length and termini. The left protomer began with Ala2 and ended with Phe185, while the right protomer began with Ser0 Met1 Ala2 and ended with Ala193. Structural changes that occurred during the simulation were described in [1]. Note that those were dynamic molecules that fluctuated with an average amplitude of ~ 0.5 Å, and we made comparison only for one of the possible (3 ns) conformational states. Figure 1 shows superposition of the simulated final 3 ns structures of the wild-type dimer and two mutant forms. It is seen that the structures generally coincide.

To characterize the structural changes, we considered the positions of C_α atoms in the main peptide chain and C_z atoms in the side groups of the largest amino acid residues Phe (11×1), Tyr (6×1), Trp (2×2), and Arg (8×1); in parentheses, there is the number of the given residues in the protomer multiplied by the number of C_z in the residue. Analysis of the C_α and C_z relative displacements along the polypeptide chain (Fig. 2) revealed three regions of large distinctions: a loop between the helix $\alpha 1$ and the structure $\beta 2$ (27–34 res., localization of mutant residue), a loop between the structures $\beta 5$ and $\beta 6$ (120–130 res.), and C-terminal amino acid residues. Since the protomers were different in length (184 and 194 res.), featured deletion Gly Asp Pro Ser Gln (123–127 res.), and did not have terminal amino acid residues Ser0, Met1, Ser191, Leu192, and Ala193, we used the alignment and changed the numbering of amino acids in the shorter protomer (left) in accordance with their numbering in the longer protomer (right)
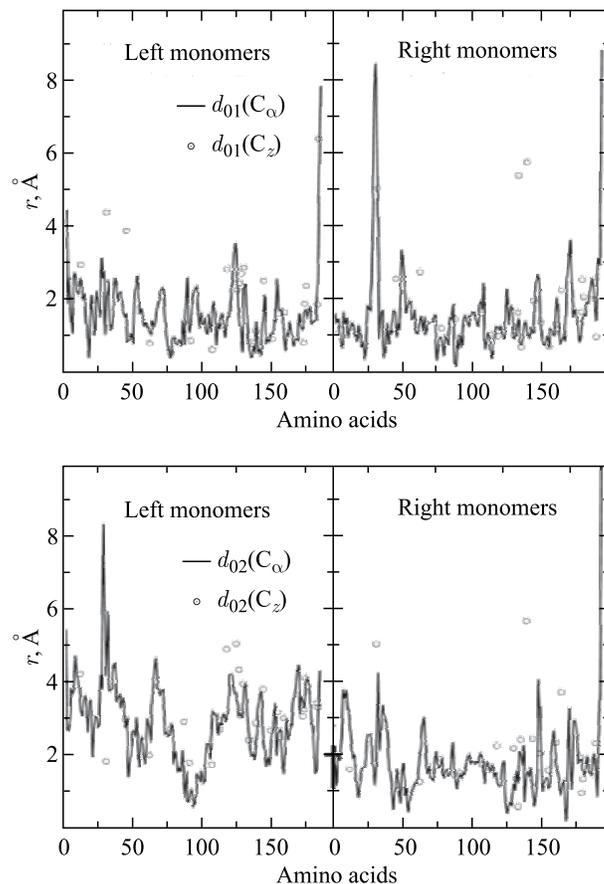
Fig. 2. Relative displacement of C_α and C_z in relax form of wild-type homodimer–mutant heterodimer ($d01$) and wild-type homodimer–mutant homodimer ($d02$). Left and right protomers are shown separately

so that the same amino acids had the same numbers. And we have always compared a short protomer with a short protomer and a long protomer with a long protomer.

In the mutant homodimer, the peptide chain core shifted much more strongly as compared with the mutant protomer in the heterodimer. The average displacement of C_α in comparison of the wild-type homodimer with the heterodimer was 1.538 (0.176–8.848), and in comparison with the mutant homodimer, it was 2.323 (0.182–10.181). As is evident from Fig. 2, displacements of C_α atoms larger than 8 Å were observed in the region of the mutant loop and at the ends

5

Left protomers   Right protomers

a   b   c   d

e   f   g   h
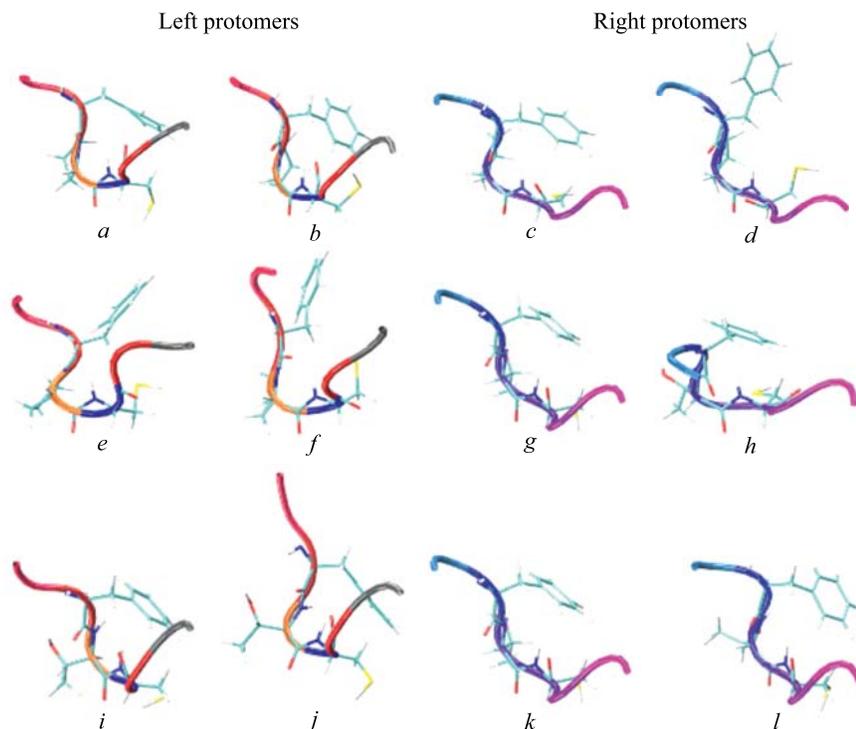
i   j   k   l

Fig. 3. Structure differences between initial and final (3 ns) states of the loop (KF[P/T]CT — res. 30–34) in wild-type homodimer ($a-d$) and mutant heterodimer ($e-h$) and homodimer ($i-l$). $a-b$, $e-f$, $i-j$ show initial and final (3 ns) states of left protomers; $c-d$, $g-h$, $k-l$ are initial and final (3 ns) states of right protomers. 1, 3 columns — initial states of the loop; 2, 4 columns — final (3 ns) states of the loop. Aromatic groups of Phe31 in different positions are shown

of the protein molecule: (left: A2, G189; right: K30, A193) in comparison with the heterodimer and (left: D29; right: A193) in comparison with the homodimer. The average displacement of C_z in comparison of the wild-type homodimer with the mutant heterodimer was 2.026 (0.490–6.397), and as compared with the mutant homodimer, the displacement was 2.637 (0.584–5.685). Displacements of C_z atoms larger than 4 Å were observed in each of the subunits in comparison of the wild-type homodimer and the heterodymer (left: F31, Y45, F188; right: F31, R133, R139) and in comparison of the wild-type and mutant homodimers (left: F12, F118, R130, F132; right: F31, R139).

Strong displacements of C_z were also found to occur in the region of the loop between $\beta5$ and $\beta6$ in comparison with the heterodimer (right: R133, R139

6

(5.8 Å)) and with the homodimer (left: F118, R130 (5.0 Å), F132; right: R139 (5.7 Å)). In the short left protomer, there was a deletion in this region (123–127 res.). But in the long right protomer the C_α core also changed (L120, S121, T122 (~ 4.2 Å)).

A comparison of the wild-type homodimer and the heterodimer (Fig. 2) showed strong shifts of the C-terminal end in both protomers (7.8 Å for Phe188 and 8.8 Å for Ala193). In the right protomer (8.4 Å for Lys30 in the $\alpha 1$ helix), when wild and mutant homodimers are compared, i.e., if protomers are in different conformations, the distance between Ala193 is large ($\sim 8-10$ Å), and if protomers are in identical conformations, the distance decreases to 4 Å. C_α atoms shifted on average by 1.7 Å at a quite narrow oscillation band. A comparison of C_α in the wild-type and mutant homodimers also showed a strong displacement of the C-terminal end but only in the right protomer (10.1 Å for Ala193), while in the left protomer a displacement of 5.1 Å was observed for Ala2.

Let us consider in more detail the changes in the region of the loop between $\alpha 1$ and $\beta 2$. Figure 3 shows conformations of the loop fragment KFP/TCN (30–34 res.) well pronounced changes in the position of the aromatic ring for the residue Phe31. A comparison of the 3 ns forms reveals strong difference in the position of the aromatic ring in two groups (d, f) and (h, j, l), whose conformations we denoted as "flip" (P) and "flop" (C).

To estimate the stability of these conformational states, we considered the position of the amino acid residues surrounding the mutant residue, namely, the distance between the carbon atom C_α of the neighboring amino acid residue Cys33 and the carbon atoms C_α and C_z of the residue Phe31 for each protomer individually (Fig. 4).

In all protomers the distance between C_α did not change and was ~ 5.5 Å, in the initial crystal form it was 5.1 Å. However, the side group of the residue Phe31 in the right wild-type protomer flipped soon after the beginning of the simulation (~ 250 ps), and the distance between Phe31 (C_α) and Cys33 (C_z) increased to ~ 9 Å, almost a factor of 2, and was maintained stable during the entire simulation process. In the left wild-type protomer of the heterodimer, the position of the side group Phe31 also changed, but at the initial point of the simulation. Maybe this change occurred during the heating stage. Then this distance of ~ 9 Å remained unchanged over the entire 3 ns simulation stage. In the mutant homodimer, the distance to the side group Phe31 changed slightly and was ~ 5.5 Å. In the region of the loop, C_z atoms in the CP-dimers shifted by 5.5 and 9.0 Å relative to the crystal, while the distance between them in the dynamic models and for the CC-conformation was ~ 5.0 and ~ 2 Å, respectively, (Fig. 2).

A strong displacement of the main polypeptide chain was also observed. In the right protomer (conformation P/C), as compared with the heterodimer, G28, D29, K30, F31, and T32 were shifted (max K30 — 8.5 Å), and in the left
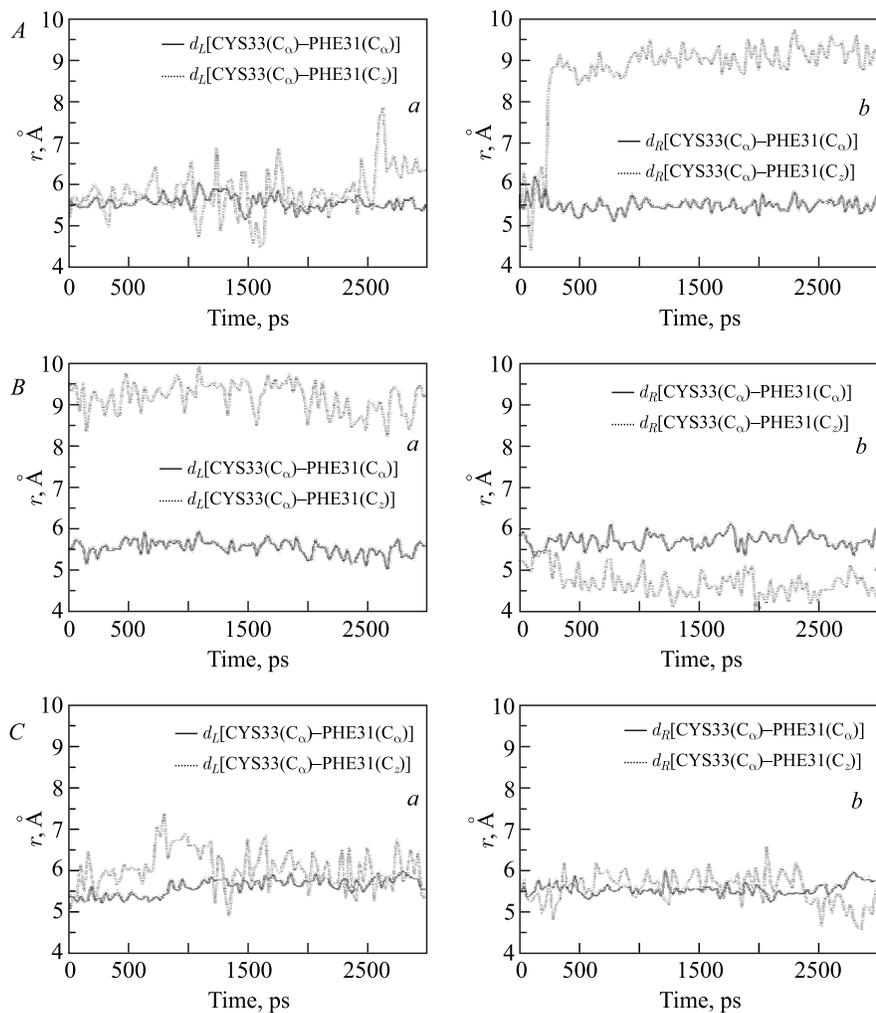
Fig. 4. Distance between Cys33 (C$_\alpha$)–Phe31 (C$_\alpha$, C$_z$) in left (*a*) and right (*b*) protomers of wild-type homodimer (P32/P32) (*A*), mutant heterodimer (P32/T32) (*B*), and mutant homodimer (T32/T32) (*C*)

protomer (conformation C/C), as compared with the homodimer, L27, D29, R30, F31, and T32 were shifted (max D29 — 8.3 Å). Note that in the left protomer of the wild-type dimer the distance was unstable and changed in the range of 4.5 to 8.0 Å. It can be assumed that the position of the neighboring residues prevents the aromatic ring from taking the equilibrium position, but further simulation can

8

lead to a "window" that will allow the protomer to take the stable P-conformation. Two other wild-type protomers took this conformation, one possibly during the heating and the other after 250 ps of the simulation.

Figure 5 depicts the position of the mutant loop and terminal sites. In phosphatase, there are α helices at the terminal ends, i.e., the terminal ends are structured. Spatially, they are localized near the mutant loop, and a change in the state of the loop can affect the position of the terminal ends. It is evident from Fig. 5 that in all three cases the terminal ends approach each other, as compared with the initial state. Note that the terminal ends in the left and right protomers are different (left: Ala2-Gly189; right: Ser0-Ala193). In the left protomer, the terminal ends are five amino acid residues shorter.
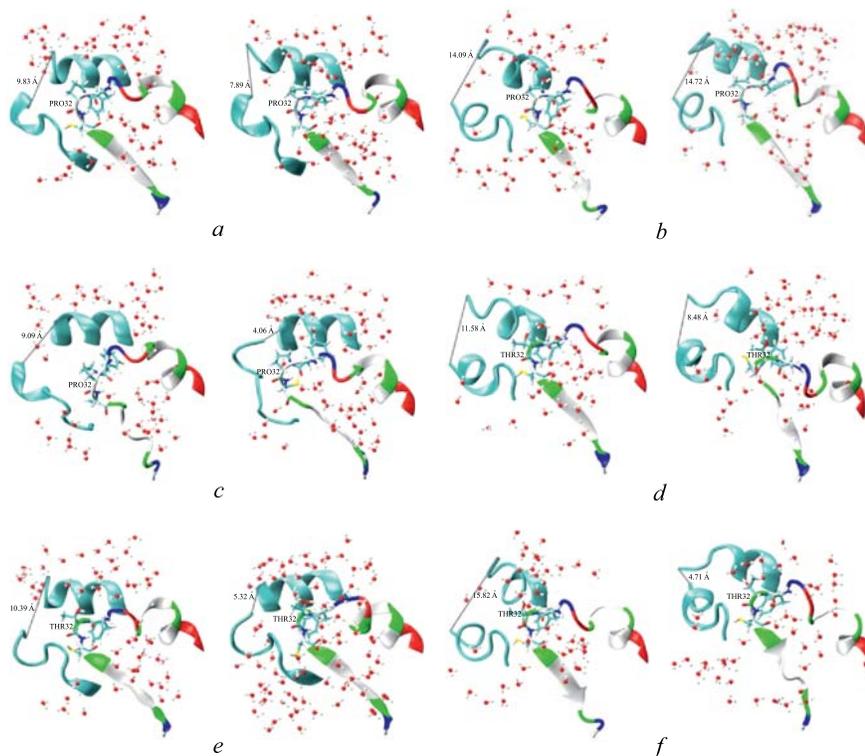

Fig. 5. Comparison of crystal and 3 ns structures of fragments of all protomers (*a*, *b* — protomers of wild-type dimer; *c*, *d* — protomers of heterodimer; *e*, *f* — protomers of mutant homodimer). Fragments include short sequences in terminal regions (10 res.) and mutant loop (20–39 res.) surrounded by the molecules of water. The distance between C_α in the first and last amino acid residues (in the left protomer between C_αAla2–C_αGly189 and in the right protomer — C_αSer0–C_αAla193) is shown

The crystal structure of the mutant homodimer (PDB: 4A95) was also obtained. Figure 6 shows superposition of the mutant apoenzyme lattice with the computer model of the mutant holoenzyme. Strong differences are observed in the region of the mutant loop. In the computer model of the holoenzyme, the loop and the $\alpha1$ helix formed by residues 16–27 were shifted to the substrate, which is a characteristic feature of the holoenzyme distinguishing it from the apoenzyme [4]. Superposition of the apoenzyme 2I5D with the enzyme of the bacteria *M. jannaschii* (2MJP, RMSD 1.3 Å) (Table 2) revealed the motion associated with the ligand binding and including the $\alpha1$ helix that incorporates residues 19 and 22 important for ligand binding. The position of Asn16, participating in the orientation of the ribose ring of the substrate, is indicated in the figure. In addition, the position of hydrophobic Phe31 is strongly different. In the crystal structure of the mutant homodimer apoenzyme, the hydrophobic residue Phe31 was seen to go into the solution [2]. However, in the computer 3 ns model the aromatic ring is oppositely directed. As a result, the hydrophobic Phe31 is inwardly directed and the polar Thr32 is outwardly directed.
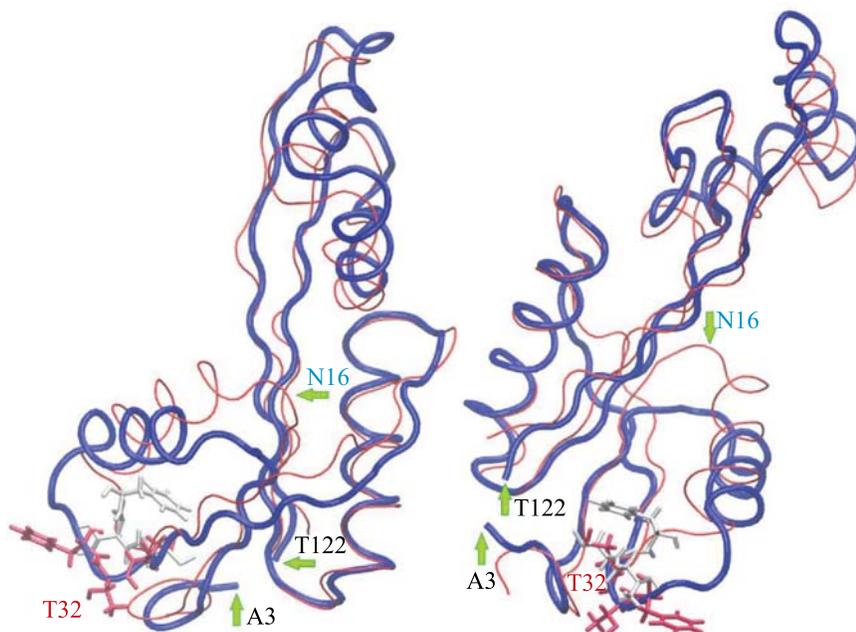

Fig. 6. Structure differences between 3 ns model on the bases of holoenzyme 2J4E and crystal (apoenzyme 4F95) of mutant homodimer P32T-*ITPA* (3–122 res.). Modeling *ITPA* is shown in red, crystal *ITPA* is shown blue. The loop containing T32 and N16 had shifted towards the active site in computing model. Thr32 was directed in opposite sides

Table 2. Comparison of RMSD$^{C\alpha}$ for crystal and modeling structures

Structures	RMSD (Å)
apo-*hITPA* 2CAR — apo *M. jannaschii* 1B78	1.500
apo-*hITPA* 2I5D — apo + substrate *M. jannaschii* 2MJP	1.300
apo-*hITPA* 2CAR — apo *hITPA* 2I5D	0.480
apo-*hITPA* 2CAR — apo + substrate *hITPA* 2J4E	—
apo + substrate *hITPA* 2J4E — apo mutant 4F95	1.400
apo + substrate *hITPA* 2J4E — comp. model wild-type	1.632
apo + substrate *hITPA* 2J4E — comp. model heterodimer	1.747
apo + substrate *hITPA* 2J4E — comp. model homodimer	1.648
comp. model wild-type — comp. model homodimer	2.323
comp. model wild-type — comp. model heterodimer	1.538
apo mutant 4F95 — comp. model homodimer	—

The volume of protomer is $51.895 \times 52.402 \times 71.343$ Å. Visualization of the water molecules in a volume of $20 \times 20 \times 20$ Å around the mutant amino acid residue allows one to estimate the situation for the side group of the residue Phe31. As is evident from Fig. 5, the number of water molecules in the loop volume and surroundings of the hydrophobic residue Phe31 did not change.

2. DISCUSSION

During the computer simulation, pyrophosphatase atoms shifted as compared with the crystal 3 ns structure; the RMSD$^{C\alpha}$ values were 1.75, 1.8, and 1.5 Å for the wild-type protomers in the wild-type homodimer and mutant heterodimer and 2.0, 2.2, and 2.3 Å for the mutant protomers in the mutant homodimer and heterodimer, i.e., the shift of the atoms was stronger in the mutant protomers. These values are comparable with the average shifts in comparison of crystal structures from different organisms (Table 2), e.g., a superposition between the human apo-*hITPA* structure (2CAR) and the bacterial *Methanococcus* enzyme (1B78) gives a root-mean-square deviation of 1.5 Å for C$_\alpha$ positions (184 aligned residues with 35% sequence identity) [4].

Earlier the superposition of wild-type and mutant apoenzyme crystal structures revealed changes in the loop between $\alpha1$ and $\beta2$ (28–33 res.), the site of localization of mutant amino acid residue Phe31-Pro32Thr-Cys33 [2]. Upon substrate binding there was an upward rigid body rotation of the $\alpha1$ helix around residues 11 and 26–32. When the two structures were superimposed, the C$_\alpha$ positions of residues 15–31 showed a root-mean-square difference of 4.8 Å between the apo- (2CAR) and ITP-bound (2J4E) enzymes [4].

11

A comparison of computer 3 ns models of the wild-type holoenzyme with the mutant dimers revealed three regions of strong distinctions: a loop between $\alpha1-\beta2$, a loop between $\beta5-\beta6$, and C-termini. Protomers in the ternary structure exhibited two stable conformations of the neighboring hydrophobic residue Phe31: "flop" and "flip". The analysis of the Phe31 position showed that "flop" conformation was typical of mutant Thr32 protomers, while "flip" conformation was typical of wild-type Pro32 protomers. For these conformations, the distance between the bordering residues Cys33 (C_α) and Phe31 (C_z) ranged between ~ 4 and 8.5 Å. The simulation was performed for 3 ns, and those conformations were stable, though they can probably change their positions in further simulation. Though both positions of phenylalanine are very different, they do not bring it beyond the interface of the simulated enzyme, unlike the case of the mutant crystal structure.

In the crystal structure of the mutant, the position of the backbone for residues near Thr32 was shifted, causing Phe31 and Thr32 to be flipped out into the solvent [2]. The C-terminus was also disordered. The side chain of Phe189 had shifted position and occupied the location of Phe31 in the wild-type structure. The remainder of the C-terminus continues along a different trajectory, although the final three residues (Leu192, Ala193, and Ala194) could not be modeled due to lack of electron density. Both N- and C-termini appear to no longer form a short α helix. Note that in this model (4F95) Met1, Ala2, Leu192, Ala193, and Ala194 were deleted due to lack of electron density.

A comparison of computer models also showed that positions of C-termini are greatly different in the wild type and the mutant. The distance between the N- and C-terminus decreased during the simulation, and the decrease was larger in the mutant protomers. However, in our simulation residues at both termini were considered and α helices were formed at both termini. The termini were localized beyond the loop and did not interfere in localization of Pro32Thr.

Thus, the computer models did not agree with the crystal models either for the wild-type or for the mutant. In the apo-*hITPA* crystal there was lack of well-defined electron density for residues in the region around Thr32 [2]. The lack of electron density indicates that it is a region of internal disorder. Such proteins have no unique tertiary structure in an isolated state and acquire it after interaction with their ligands. Regions of internal disorder are typical for polyfunctional proteins with several substrates that have to adapt to the substrates. Indeed, pyrophosphatase has high affinity for several substrates (ITP, dITP, XTP), and the active site thus has to adapt to them. This is possible due to flexibility of the loop between $\alpha1$ and $\beta2$ in orientation, for example, of the $\alpha1$ helix and Arg16 that participates in substrate binding. It is probable that the loop was structured during the binding with ITP. Mutation of P32T affects the structure of the loop and can affect the activity of the enzyme and affinity for substrates. The crystal structure of the mutant apoenzyme exhibits internal disorder [2] but wild-

type apoenzyme does not (Yu. I. Pavlov, personal communication); unfortunately, the description of the holoenzyme crystal has no information on whether there are regions with lower electron density. Further investigations, e.g., analysis of holoenzyme structures with different ligands are needed for understanding these processes.

A concordant idea about a mechanism for catalytic deficiency in P32T mutant *ITPA* was suggested [4]. Comparison of two crystal structures (apo and holo) shows that lobe movement and rearrangement of the $\alpha1$ helix are responsible for nucleotide exchange. Located in the hinge region of the flexible $\alpha1$, Pro32 is a key residue for positioning of the side chains involved in substrate binding and catalysis. But they suggested that a disturbed nucleotide exchange or a partial misfolding of the $\alpha1$ helix is likely to be transmitted across the dimer interface, rending the dimer inactive, e.g., influence on dimer formation.

In addition, we observed oscillatory motion of the enzyme structure with amplitude of ~ 0.5 Å and a period of ~ 1 ns. It can be assumed that the oscillatory motion facilitates substrate binding and disposal of PP and IMP reaction products.

Apart from the mobility of the loop and the shape of the enzyme (holoenzyme with the ITP substrate was simulated, the flop conformation of the apoenzyme without substrate was crystallized), the differences observed in the structures of the crystal and simulated enzyme probably arise from the conditions in which the enzyme was. Our simulation was performed in water environment (27°C, pH 7), and crystallization conditions were also suboptimal for catalysis with respect to pH and temperature (buffer 150 mM NaCl, pH 8.5, 25°C); *in vitro* reaction optimum is pH ~ 10.

In addition to the loop where the mutation is localized, other regions of strong changes were revealed. For example, when comparing the simulated structures, we observed strong shifts in the region of loops $\beta5$ and $\beta6$. Other authors also showed that in the case of superposition of C_α between the human crystal apoenzymes 2CAR and 2I5D obtained in different laboratories the RMSD was 0.48 Å, with the greatest differences (> 5 Å) in loop 124–127 between sheets $\beta5$ and $\beta6$ (Porta et al., 2006). When this loop was removed from the superposition, the $RMSD^{C_\alpha}$ was only 0.2 Å.

Thus, structural changes caused by the Pro32Thr mutation were found in the computer models. However, further investigations are needed for clarifying functional consequences of these changes.

REFERENCES

1. Dushanov E. B., Kholmurodov Kh. T., Koltovaya N. A. *Biophysics*, 2015, **60**, 529–537.
2. Simone P. D. et al. *J. Struct. Biol.*, 2013, **182**, 197–208.
3. Bierau J., Lindhout M., Bakker J. A. *Pharmacogenomics*, 2007, **8**, 1221–1228.
4. Stenmark P. et al. *J. Biol. Chem.*, 2007, **282**, 3182–3187.
5. Stepchenkova E. I. et al. *J. Mol. Biol.*, 2009, **392**, 602–613.
6. Marinaki A. M. et al. *Nucleosides, Nucleotides and Nucleic Acids*, 2004, **23**, 1399–1401.
7. Herting G. et al. *Biochem. Biophys. Acta*, 2010, **1802**, 269–274.
8. Porta J. et al. *Acta Cryst. Section F. Struct. Biol. Crystal. Commun.*, 2006, **62**, 1076–1081.
9. Savchenko A. et al. *J. Mol. Biol.*, 2007, **374**, 1091–1103.
10. Joint Center for Structural Genomics, 2011, DOI:10.2210/pdb1vp2/pdb.
11. Lokanath N. K. et al. *J. Mol. Biol.*, 2008, **375**, 1013–1025.
12. Hwang K. Y. et al. *Nat. Struct. Biol.*, 1999, **6**, 691–696.
13. Abergel C. *Acta Cryst. Section D*, 2013, **69,** 2167–2173.
14. Sayle R. A., Milner-White E. J. *Trends in Biochem. Sci.*, 1995, **20**, 374–376.
15. Koradi R., Billeter M., Wuthrich, K. *J. Mol. Graphics*, 1996, **14**, 51–55.
16. Humphrey W., Dalke A., Schulten K. *J. Mol. Graphics*, 1996, **14**, 33–38.

Редактор *Е. И. Крупко*